

Integrated Launch Package Performance in the Cannon-Caliber Launcher

Alexander E. Zielinski, Keith Soencksen, David W. Webb, and Paul Weinacht
U.S. Army Research Laboratory (ARL), Aberdeen Proving Ground (APG), MD 21005-5066

Abstract—The Cannon-Caliber Electromagnetic Gun (CCEMG) Program is a major effort toward proving the viability of electromagnetic weapons for future use by the Armed Forces. The effort is focused on the successful, system-designed integration of several major components. Crucial to the success of the program are the operational characteristics of the launcher and the integrated launch package (ILP). This paper addresses the launch and flight characteristics, accuracy, and terminal performance of the ILP and subprojectile. The results presented here represent the first known experimental assessment of these parameters obtained from electric gun firings of a tactical flight body over realistic ranges.

To date, 39 shots have been fired using a 1.6-MJ capacitor bank located at the U.S. Army Research Laboratory (ARL). A wide variety of instrumentation was incorporated to survey transitional, free-flight, and terminal ballistic regimes from the gun muzzle to target impact 222 m downrange. Free-flight aerodynamic data indicated that the round has adequate in-flight stability. Round-to-round dispersion was computed over a wide range of launch velocities based on downrange impact locations and was used to provide estimates of the dispersion at the design launch velocity of 1,850 m/s. A detailed analysis of the transitional ballistic process has been performed to quantify the various contributors to the total launch disturbance. The results indicated that the sabot/armature discard contributes equally with the aerodynamic jump toward target impact dispersion and increases with launch velocity. For the current launcher configuration, the variability of the discard process is oriented in the vertical direction. Finally, impact data on armor were limited but nonetheless indicate the round is capable of meeting the CCEMG system requirements.

I. INTRODUCTION

The Cannon-Caliber Electromagnetic Gun (CCEMG) Program is jointly sponsored by the U.S. Army Armament, Research, Development, and Engineering Center (ARDEC) and the U.S. Marine Corps (USMC). The effort brings together technologies necessary to demonstrate the potential for a medium-caliber weapon system. Presently, the work is in the final stages of component integration and system testing. Specifically, the University of Texas, Center for Electromechanics (UT-CEM), is tasked with the launcher and armature development [1], [2], and Kaman Science Corporation (KSC) is tasked with the development of the Integrated Launch Program (ILP) [3]. The U.S. Army Research Laboratory (ARL) was tasked with assessing single-shot performance

Manuscript received April 8, 1996.

A. Zielinski, e-mail: zielinsk@arl.mil, or fax: 410-278-2460; K. Soencksen, e-mail: soenckse@arl.mil; D. Webb, e-mail: webb@arl.mil; and P. Weinacht, e-mail: weinacht@arl.mil.

of the launcher and ILP. The series-augmented launcher is 2.25 m long and has a rectangular bore cross section (17.3 mm \times 39 mm). The ILP weighs 180 g (90-g armature, 90-g subprojectile) and is designed to operate at 1,850 m/s. The armature is a two-piece design with the separation plane in the vertical direction. The subprojectile length is nominally 175 mm with the center of gravity (cg) 85 mm behind the nose. A developmental approach has been taken, and, in this paper, we discuss single-shot experimental results in support of achieving the CCEMG system requirements [4]. A photograph of a recently tested ILP is shown in Fig. 1.

The organization of this paper is as follows: In Sec. II, the experimental conditions are described. In Sec. III, we describe the acquisition of the aerodynamic data and their use in evaluating the models. In Sec. IV, we compute the target impact dispersion and mean impact location. In Sec. V, ILP jump is described and its components evaluated. In Sec. VI, the terminal ballistic performance is discussed. Finally, Sec. VII contains our summary.

II. EXPERIMENT

A capacitor bank was used to provide energy to the launcher. To operate at high-peak current with the capacitor bank, a switch was incorporated at the muzzle and is time-delayed to close just prior to projectile exit. When the muzzle switch is triggered, the current falls to near-zero in roughly 0.5 ms. A representative current trace for the launcher (solid line) and muzzle switch (dashed line) currents is shown in Fig. 2. For this shot, the initial charge voltage is 8.6 kV, and the muzzle switch was closed at 1.63 ms. The ILP exits the launcher at 2.16 ms with a muzzle velocity (MV) of 1,639 m/s. For shots that did not use the muzzle switch, the launcher current is equal to the armature current, and the current at projectile exit is larger than the value reported here. Other electrical data acquired during the shot include the breech, launcher, and muzzle voltages. The electrical performance of the launcher is presented elsewhere [1]. The launcher was firmly bolted to a steel frame at the breech end and supported 0.6 m from the muzzle end. The steel support frame was bolted to steel channel imbedded in the concrete floor.

Data for two ILPs are considered in the program: (1) a six-fin fluted-flare-stabilized round and (2) a four-fin swept-delta configuration. The six-fin subprojectile was tested with the baseline armature design (shots 10–16) while a modified armature was tested with the four-fin configuration (shots 17–39).

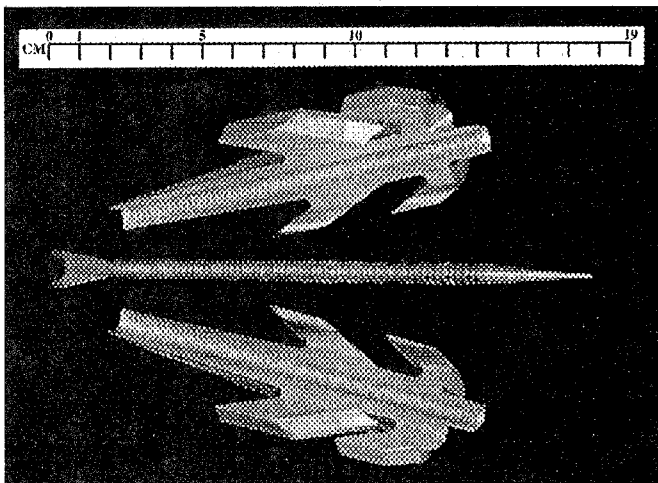


Fig. 1. Photograph of recently tested ILP.

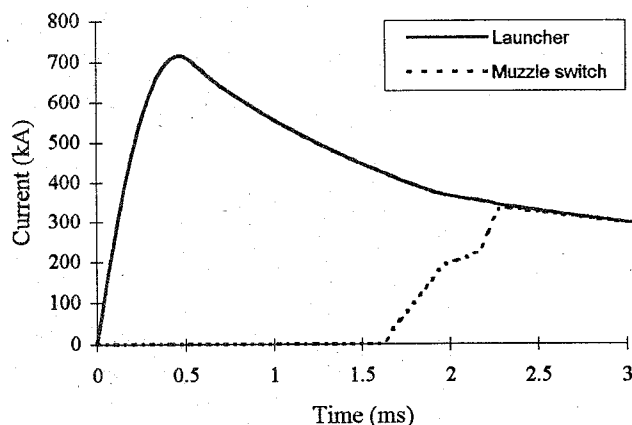


Fig. 2. Launcher and muzzle switch currents from shot 38.

A number of measurement techniques were used to assess launch velocity. Measurements based on the time rate of change of the armature's induction field (dB/dt) at the muzzle are within 4% of smear camera, flash x-ray, radar, and break screen techniques. All velocities reported in this paper are inferred from dB/dt signals.

For the evaluation of launch dynamics, an aim point and intended line of flight (LOF) were established by using a boresight and mount. A pulley was securely fastened 10 m downrange and aligned with the boresight crosshair. A cable was attached at the breech, pulled through the muzzle, and suspended over the pulley with 50 kg. The cable, for indicating LOF, and beads, for referencing the subprojectile cg location, were superimposed upon each x-ray.

Yaw cards (cardboard targets) were consistently used to assess the free-flight aerodynamics of the projectile. As many as 15 yaw cards were placed at measured intervals along the trajectory. After each shot, the horizontal and vertical dis-

placements of the flight body from the original aim point as well as its angle of attack (AoA) produced by the pitching and yawing motion were measured from the impact on the yaw card. In the absence of x-rays, yaw cards were often used to qualitatively evaluate the sabot discard. Accurate placement of the aim point on the yaw cards was possible using the boresight and mount. Horizontal and vertical lines were also marked.

At the initiation of hardware testing at ARL, the flight range was limited to 30 m. As the results became encouraging, range testing was extended to 222 m. The topology of the terrain was also a factor in incorporating instrumentation. A 5-m-wide \times 5-m-high \times 20-mm-thick steel plate was used as an impact target. For shots 28–39, a high hard armor (HHA) target was placed in front of the impact target to acquire penetration data.

III. FREE-FLIGHT DATA AND ANALYSIS

The free-flight performance of the subprojectile is determined by two factors: (1) the aerodynamic performance of the subprojectile and (2) the disturbances to the subprojectile during the launch and sabot discard process. The measured angular motion was fit to a theoretical model of the yawing motion, which is based on an analytical solution of the yawing motion of a rolling symmetric missile [5]. For a nonrolling, statically stable missile, the analytic solution indicates that both the horizontal and vertical yawing motion can be modeled as a damped sinusoidal motion with the same frequency and damping rate, but possibly different initial amplitudes and phase angles. Fits are also possible with positive and negative damping. A nonlinear, least-squares fitting process was utilized to fit the measured angular orientations to the theoretical motion to obtain the six independent parameters (two initial amplitudes, two phase angles, one frequency, and one damping rate) for most of the shots.

The frequency and damping rate of the yawing motion are purely functions of the aerodynamic and mass properties of the body, and thus can be predicted using theoretical aerodynamic approaches such as computational fluid dynamics (CFD). A parabolized Navier-Stokes (PNS) approach [6] was utilized to predict the aerodynamic performance of the subprojectile prior to the experimental testing. The theoretical results supplemented the experimental measurements since the yaw card data provide only a limited set of aerodynamics.

From the measured yawing frequency, an important measure of the projectile's static stability, the pitching moment coefficient ($C_{m\alpha}$), was extracted and compared with the predictions. In Fig. 3 the coefficient is plotted as a function of launch velocity for AoA magnitudes less than 10° . In general, good agreement is found, and the results show a decrease in the subprojectile's stability with increasing velocity due to the decreased efficiency of the fins at higher velocity. Data from one of the six-fin fluted-flare firings (shot 15) is included and show the improvement in aerody-

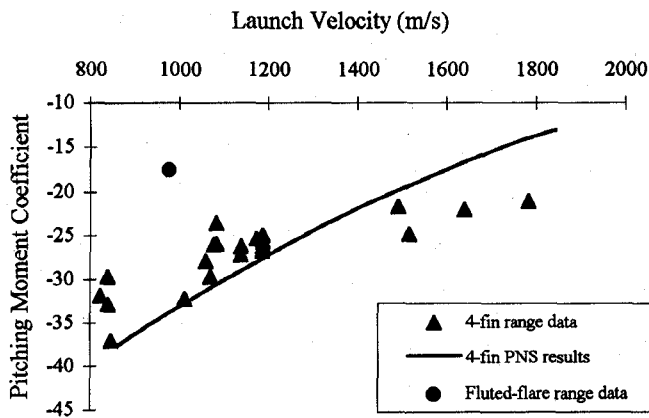


Fig. 3. Pitching moment coefficient ($C_{m\alpha}$) as a function of launch velocity.

dynamic performance of the subprojectile obtained by changing from the fluted-flare to the finned afterbody. Both the experimental data and theoretical predictions indicate that the aerodynamic damping performance of the body will cause the amplitudes of the yawing motion to damp to less than 10% of their initial amplitudes after 500 m of flight.

On a few shots after shot 27, radar was used to obtain the round's velocity as a function of range. From this data the subprojectile's retardation and drag coefficient were obtained. Comparisons between predicted and measured drag coefficients are shown in Fig. 4. Also included is a data point from a subscale firing at the ARL Aerodynamics Range (solid circle) [7] as well as PNS prediction for the subscale projectile. The theoretical approach is a reasonable assessment of the expected performance of the subprojectile. The results indicate that the velocity of the projectile will decrease at a rate of 150–200 m/s/km.

IV. DISPERSION AND ACCURACY

The variability of impact locations on a target is called the round-to-round dispersion. In weapon systems analysis, dispersion measures the precision of fire, and large values can significantly degrade a weapon system's lethality. In this section, we consider all impact points in the projectile's flight path to assess dispersion.

The data consisted of downrange impact locations in azimuth and elevation measured in mils.¹ The impact data for 21 shots using the four-fin configurations were evaluated as a function of MV. Shots were categorized as either low (825–850 m/s), medium (1,000–1,200 m/s), or high (1,275–1,800 m/s) MV. Additionally, medium MV shots were partitioned into two subgroups, according to whether or not the bore was honed between shots.

¹ 1 mil equals 1 m at 1,000-m range.

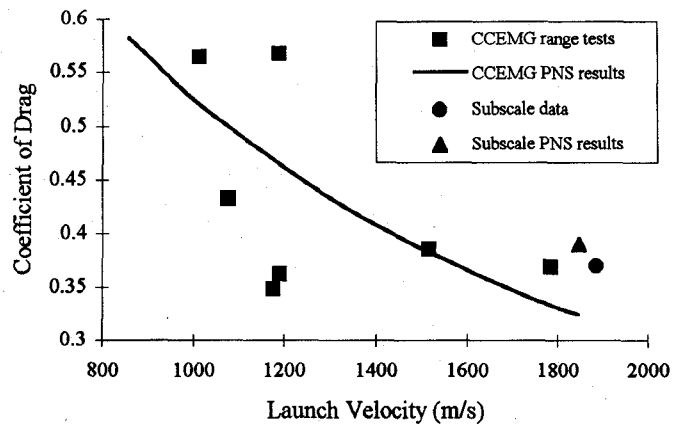


Fig. 4. Coefficient of drag (C_D) as a function of launch velocity.

Computation of dispersion at any target (yaw card or armor) requires the impact locations of at least two rounds. Within the same shot group, the round-to-round dispersion estimates at each downrange target were pooled to obtain a more stable, overall estimate of dispersion. This pooled estimate was also weighted by target distance, so that farther targets, where the transients from launch have diminished, have greater influence on the calculated dispersion. The formula for each group's pooled round-to-round dispersion estimate, s_p , is

$$s_p = \sqrt{\frac{\sum d_i(n_i-1)s_i^2}{\sum d_i(n_i-1)}} \quad (1)$$

where d_i is the distance to target i , n_i is the number of rounds that impacted target i , and s_i is the round-to-round dispersion estimate at target station i .

In Fig. 5, we plot the round-to-round dispersion estimate as a function of the average MV for each of the four shot groups. In both directions, dispersion increases as a function of MV. While it is mathematically possible to perform a linear regression analysis on these data to obtain extrapolated estimates of dispersion at 1,850 m/s, such an approach is not recommended for two reasons. First, the error of prediction when using such a small number of points is usually very high. Second, the high MV group spans a wider range of muzzle velocities than all other rounds from the other three groups. All information concerning the relationship between MV and dispersion in the 1,200-m/s to 1,800-m/s range is lost when the data are condensed to a single point.

As an alternative approach, each of the four shot groups was partitioned into smaller groups, thus generating more points for the plot of average MV vs. dispersion. The analysis considered all possible partitions of sizes 2 and 3 within each shot group. When forming the partitions, we imposed the restriction that no partition could contain shots with muzzle

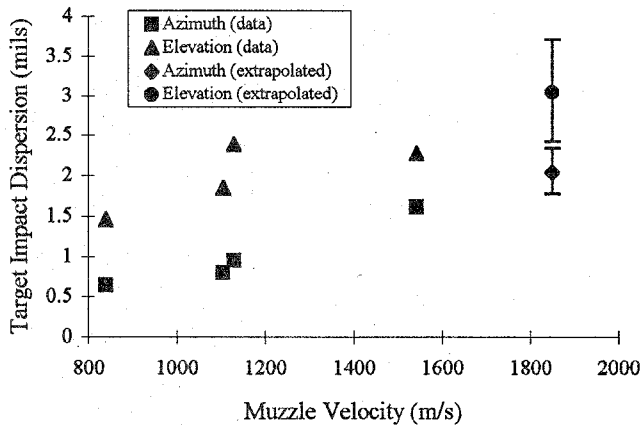


Fig. 5. Round-to-round dispersion in azimuth and elevation (confidence intervals are indicated at 1,850 m/s).

velocities differing by more than 270 m/s. Under this rule, 1,890 distinct rearrangements of the data are subjected to a weighted linear regression. This analysis strategy produces a collection of dispersion estimates at 1,850 m/s instead of a single value. Using the 5th and 95th percentiles of these 1,890 values, one obtains 90% confidence intervals. These intervals are (1.8, 2.3) mils in azimuth and (2.4, 3.7) mils in elevation and are indicated in Fig. 5 along with the median values of 2.0 mils in azimuth and 3.0 mils in elevation.

The accuracy of the subprojectile is measured by its impact location relative to the aim point. The subprojectiles tend to impact to the left of the aim point and are scattered about the aim point in the vertical direction. However, the muzzle velocity and impact location data do not suggest a linear trend between these two variables in either direction. Statistical regression analysis confirms this observation. Therefore, regardless of launch velocity, the estimated impact is given by the means of the data, namely -1.2 mils in azimuth and 0.2 mils in elevation.

V. JUMP

A) Jump Description

The trajectory, and hence the dispersion, is influenced by the series of launch disturbances leading up to free flight. In this section, we discuss the series of six disturbances from shot start to the impact of the round at the target (TI). Jump is a vector, the sum of whose horizontal and vertical components are equal to the linear deviation from the line of fire from forces acting on the ILP. The first component is the pointing angle of the muzzle at projectile exit (PA). At the same time, the muzzle experiences a transverse velocity that is imposed upon the projectile (CV). The third component is the angular deviation of the projectile cg from the instantaneous bore centerline at projectile exit (CG). The next

component is the net deviation due to sabot discard disturbances (SD). The fifth jump component is the aerodynamic jump (AJ). The final jump component is the gravity drop (GD). Each jump component has a dispersion associated with it. A thorough discussion of projectile jump and its measurement can be found in [8].

B) Component Determination:

Instrumentation was not available to monitor the dynamic motion of the muzzle. However, the aim point of the launcher relative to the 222-m target was checked periodically and found not to change between shots. In this paper, we assume that CV and PA vectors are negligible. The CG vector is determined from location of the round's cg from the fiducial in the multistation orthogonal x-rays. A straight line is fit to the cg locations as a function of range for each plane and the slope of the line is the CG vector.

The AJ component originates from angular rates produced near the muzzle. These rates cause a linear deviation of the mean flight trajectory from the original line of fire. A reasonable approximation [5] is given as

$$AJ = \frac{I_t C_{L\alpha}}{md^2 C_{m\alpha}} (\dot{\omega}). \quad (2)$$

The subprojectile moment of inertia (I_t), diameter (d), and mass (m) were measured. $C_{L\alpha}$ and $C_{m\alpha}$ are obtained from CFD computations. The angular rate ($\dot{\omega}$) for each plane was determined using the CFD value for $C_{m\alpha}$; and the peak angles (ω_o) and period (T) were obtained from the fits to the yaw card data as:

$$\dot{\omega} = 2\pi\omega_o/T. \quad (3)$$

In this paper, we compute the SD vector as the vector required to close the jump diagram between the CG component and the AJ component. Lastly, the GD component has been computed from the launch velocity and accounted for in each yaw card and target impact location.

Fig. 6 shows a three-component jump vector diagram using impact data at 30 m downrange for shot 24. The three components evaluated are CG, SD, and AJ. The aim point is located at (0,0), and the impact at the target is denoted TI. In shots where multistation orthogonal flash x-rays were not available, a launch dynamics (LD) vector was constructed from the origin to the AJ vector. The LD vector contains the combined effects of CG and SD. Similar plots were made for all the shots. Once the jump vector diagram is assembled, each vector is referenced from the origin. The variability of the vectors for each component is computed as the component dispersion.

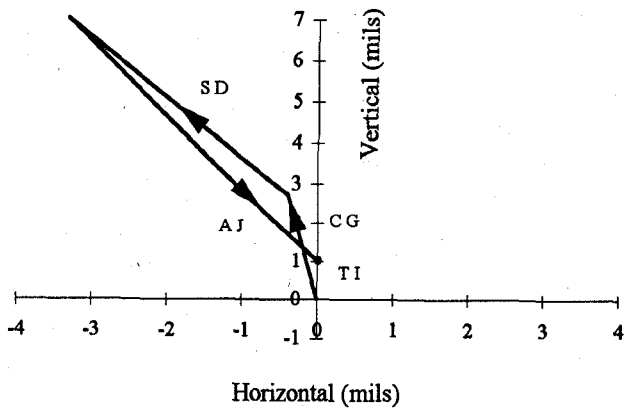


Fig. 6. Jump vector diagram for shot 24.

C) Jump Survey

The angular rates determined by the x-rays are indicative of the in-bore balloting forces and bore centerline acting on the ILP cg. The angular rates associated with free flight are also a result of the armature discard event and represent the final angular motion of the round. In Fig. 7, the fitted free-flight yawing motions and the angles as measured in the x-rays for the six-fin configuration are plotted as a function of range. There were no aerodynamic features incorporated on this armature to ensure reliable separation. It is clear that close to the muzzle but before the armature begins to discard, the yawing motion is approaching 5° , according to the x-ray data. However, shortly after the second x-ray station, the armature separates from the round and the angular rates have changed significantly. By 5 m, the impulse associated with the armature discard has begun to manifest itself as a larger angle as the round begins to enter free-flight. Because of the large angles associated with this shot, the effect of the discard was obvious. Subsequent design changes (shots 17–39) to the separation scoop and rod-armature interface resulted in improved discard.

The angular rates for the velocity groups 826 m/s and 1,126 m/s are comparable in magnitude. In all cases, the magnitude of the free-flight rates are noticeably larger than those measured by the x-rays. This suggests the discard event is able to couple enough force to alter the round's angular rate just as it enters free flight. On average, 63% of the magnitude of this disturbance is oriented in the vertical direction. It is suspected that the increased disturbance in the vertical direction is initiated by the armature discard disturbance in the plane of separation (i.e., horizontal direction) and transformed through the downward rotation of the armature halves into a disturbance in the vertical direction. In the time interval between the ILP disengagement from the launcher and completion of armature discard, initial angles and angular rates are

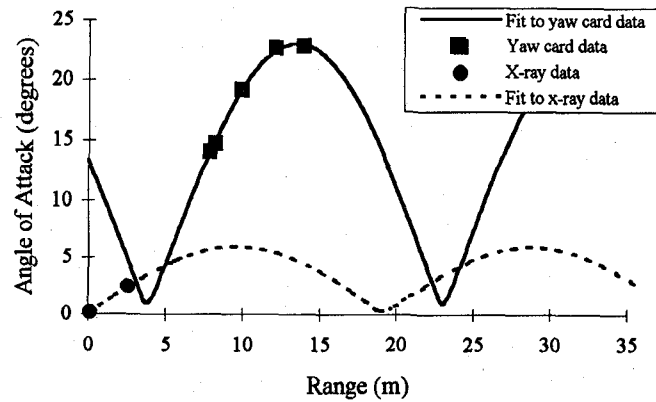


Fig. 7. Fitted free-flight (solid line) and muzzle (dashed line) AoA for shot 16. Symbols indicate measured data.

established in the ILP. For the first 3.5 m and over a wide range of velocities, the front of the armature has moved less than a few rod diameters away from the body of the rod. Also, the rear of the armature has not started to move away from the rod body until 2.5 m downrange. After 4 m, the slope of the displacement data dramatically changes as the discard event proceeds. The location of each armature half varies very little as a function of range despite the widely varying velocities, exit currents, and initial conditions.

In Fig. 8, we plot the dispersion for the AJ and LD components as a function of average launch velocity for shots 17–39. The discontinuity in the plot at 1,100 m/s is at a point in the testing where minor revisions were made to the armature. The component dispersion is larger in the vertical direction than in the horizontal direction, and the dispersion increases more rapidly for the vertical direction. This trend was also seen in the dispersion. The dispersion for the launch dynamics and aerodynamic jump components is roughly the same in each plane.

If we assume the CG measurements obtained on shots 20 and 24–27 are unknown, then we can compute an equivalent LD vector and corresponding dispersion for those shots. The dispersion at 1,126 m/s for the equivalent LD vector is 1.00 mil in the horizontal plane and 2.28 mils in the vertical plane. For the two components that constitute the LD vector, namely, CG and SD, we find that the SD contribution towards the LD vector is greatest. Also the SD dispersion component increases with velocity.

Finally, all the CG vectors were oriented above and to the left of the LOF. The measured deviation from the launcher centerline (i.e., straightness) at the muzzle and the mean impact location are also oriented in the same directions. These data suggest that this launcher has an interior ballistic dynamic path that consistently launches the ILP with this bias.

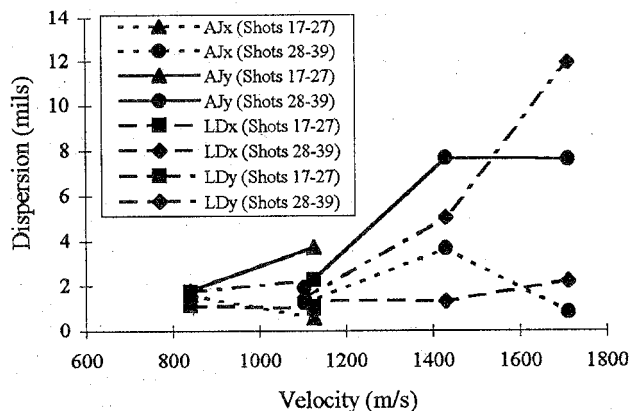


Fig. 8. Dispersion for jump components as a function of average launch velocity.

VI. TERMINAL PERFORMANCE

Penetration requirements for CCEMG are given in [4]. After shot 27, an HHA target assembly was placed down-range just ahead of the steel impact target. A yaw card was placed directly in front of the HHA target to monitor the AoA at impact. Five out of 11 rounds hit the HHA target, producing 3 partial penetrations and 2 perforations. We have used these data to compute an effective value of armor penetration from the combined HHA and steel [9]. The fit to the data with the measured retardation suggests that the round is capable of meeting the penetration-at-range requirements.

VII. SUMMARY

Results indicate strong potential for a medium-caliber weapon system. The ILP has been launched successfully at 96% of its design velocity. This represents 86% of the expected peak axial acceleration. Instrumentation including radar, orthogonal flash x-ray units, smear and high-speed cameras, and yaw cards was successfully incorporated as part of the test matrix and proved useful in diagnosing the ILP behavior. Shots were performed where the bore was not honed or cleaned between shots, and the dispersion is identical to that obtained in the five shots where the bore was honed between shots.

The results from the jump survey indicate the individual components and dispersions can be managed with further engineering. For example, the aerodynamic jump portion of dispersion can be decreased simply by increasing the fin area of the subprojectile afterbody. Some part of the sabot discard disturbance can be minimized through quality control on the ILP tolerances.

The component of dispersion related to the centerline of the launcher (CG) appears to be minor relative to the remain-

ing components. The aerodynamic jump and sabot discard dispersion components contribute towards target impact dispersion and are nearly equal in each plane. A majority of the sabot discard component is located in the vertical direction. It is believed that these forces originate in the plane of sabot separation. The electrodynamic features associated with launcher disengagement can be a potential source affecting sabot discard. Inefficient aerodynamic features also contribute. Minimizing the magnitude of the disturbance as well as the length of interaction between the subprojectile and the armature will lead to decreased dispersion.

The quality of the armature discard and flight dynamics was improved upon by jointly redesigning the ILP with KSC. Successful implementation of range instrumentation was paramount to diagnosing the discard event. In summary, ARL was the first and only U.S. electric gun facility to launch, fly, and impact a tactical projectile configuration on target and at significant range.

ACKNOWLEDGMENT

Funding for this effort was provided by ARDEC, USMC, and ARL. Significant contributions, in support of the experimental results, were made by Mr. Ken Paxton, Mr. Steve Niles, and Mr. Barry Hudler. The assistance of Mr. Timothy Farrand in the assessment of the terminal ballistic data is greatly appreciated.

REFERENCES

- [1] A. E. Zielinski, M. D. Werst, and J. R. Kitzmiller, "Rapid fire railgun for the cannon-caliber electromagnetic gun system," presented at the IEEE Pulsed Power Conference, June 1995.
- [2] J. H. Price, et al. "Discarding armature and barrel optimization for a cannon caliber electromagnetic launcher system," *IEEE Trans. Magn.*, vol. 31, January 1995.
- [3] T. E. Hayden, R. Dethlefsen, and J. H. Price, "Effective launch package integration for electromagnetic guns," *IEEE Trans. Magn.*, vol. 31, January 1995.
- [4] J. R. Kitzmiller, et al. "Optimization and critical design issues of the air core compulsator for the cannon-caliber electromagnetic launcher system (CCEML)," *IEEE Trans. Magn.*, vol. 31, January 1995.
- [5] C. H. Murphy, "Free flight motion of symmetric missiles," Report No. 1216, U.S. Army Ballistic Research Laboratory, Aberdeen Proving Ground, MD, July 1963.
- [6] P. Weinacht and W. B. Sturek, "Navier-Stokes predictions of static and dynamic aerodynamic derivatives for high L/D finned projectiles," AGARD Conf. Proc., AGARD-CP-493, Paper 20, April 1990.
- [7] P. Plostins, K. P. Soencksen, A. E. Zielinski, and T. Hayden, "Aeroballistics evaluation of kinetic energy penetrators for electromagnetic gun applications," AIAA 96-0454, presented at the 34th Aerospace Sciences Meeting and Exhibit, Reno, NV, 15-18 January 1996.
- [8] P. Plostins, I. Celmins, and J. Bornstein, "The effect of sabot borerider stiffness on the launch dynamics of fin-stabilized kinetic energy ammunition," AIAA-90-0066, presented at the 28th Aerospace Sciences Meeting, January 1990.
- [9] E. Rapacki, K. Frank, R. Leavy, M. Keele, and J. Prifti, "Armor steel hardness influence on kinetic energy penetration," presented at the 15th International Symposium on Ballistics, Jerusalem, May 1995.